ELSEVIER

Biochimica et Biophysica Acta 1190 (1994) 57–71

BBA Biochimica et Biophysica Acta

Cation effluxes associated with the uptake of TPP^+, TPA^+, and $TPMP^+$ by *Neurospora*: evidence for a predominantly electroneutral influx process

Clifford L. Slayman *, Hideyo Kuroda [1], Antonio Ballarin-Denti [2]

Department of Cellular and Molecular Physiology, Yale School of Medicine, 333 Cedar Street, New Haven, CT 06510, USA

(Received 23 August 1993)

Abstract

Previously observed anomalies in the transport of lipid-soluble cations (LSI's) – presumed voltage-probe ions – by intact fungal cells [1] prompted a systematic investigation of ion exchanges induced by high (millimolar) concentrations of the particular species tetraphenylphosphonium ion (TPP^+), tetraphenylarsonium ion (TPA^+), and triphenylmethylphosphonium ion ($TPMP^+$). With low extracellular free Ca^{2+} (no calcium added to the medium), influx of the LSI's was biphasic, indicating rapid entry into the cytoplasm followed by sequestration into a subcompartment. The latter process, especially, was strongly inhibited by extracellular Ca^{2+} (1 mM). Contrary to the expectation for electrophoretically driven entry of LSI's into fungal cells, no major efflux of protons (acidification of the medium) could be measured; in fact, significant alkalinization of the medium was observed. The major cellular inorganic cations, K^+ or Na^+ (under different conditions), were released during LSI uptake, but with kinetic behavior which clearly ruled out direct coupling to the uptake of TPP^+, TPA^+, or $TPMP^+$. The major mechanism for entry of these lipid-soluble cations into *Neurospora* appears to be electroneutral diffusion in combination with one or more hydrophilic anions. Subsequent penetration of the fungal vacuoles would result in binding of LSI's to storage polyanions (viz., polyphosphate) and concomitant displacement of the normal vacuolar cations, such as basic amino acids and polyamines, thus leading to alkalinization of the extracellular medium. The observed effluxes of cytoplasmic K^+ and Na^+ should result independently from energetic changes (i.e., uncoupling of the mitochondria) and are most easily described by simple, but asynchronous, changes in the average rate constants for entry and exit of the alkali-metal cations.

Key words: Tetraphenylphosphonium ion (TPP^+); Tetraphenylarsonium ion (TPA^+); Electroneutral diffusion; Lipid-soluble ion; Ion compartmentation; (Fungus)

1. Introduction

In the previous paper [1] it was shown that small lipid-soluble cations (LSI's), such as tetraphenylphosphonium (TPP^+) and tetraphenylarsonium (TPA^+), used at low concentrations (≤ 100 μM), do not distribute to equilibrium with the plasma membrane voltage in *Neurospora crassa* or *Saccharomyces cerevisiae* under any reasonable circumstances: e.g., over intervals of minutes to tens of minutes, in intact cells which are actively metabolizing. The observation vitiates the use of such ions as membrane voltage probes in these species, and raises serious questions about their use in all 'walled' eukaryotic cells. (Validation of these same agents as membrane voltage probes in certain animal cells and Gram-positive bacteria has been discussed [1].)

Three aspects of the results were of particular interest. First, intracellular sequestration did not play a critical role, since calculated average internal concentrations (estimated by measuring depletion from the medium) were much too small – appropriate for membrane voltages positive to -90 mV, compared with directly measured voltages negative to -180 mV. Second, in tests made at moderate or high concentrations

* Corresponding author. Fax: +1 (203) 7855535.
[1] Current address: Department of Biology, Toyama University, 3190 Gofuku, Toyama-City 930, Japan.
[2] Current address: Dipartimento di Fisiologia delle Piante e Chimica Agraria, Universitá di Milano, Via Celoria 2, 20133 Milano, Italy.

SSDI 0005-2736(93)E0325-5

of TPP^+ or TPA^+ (1–30 mM) roughly parallel membrane depolarization and ATP depletion were observed, but such effects were greatly diminished by repeated washout and retesting of the lipid-soluble ions, or even by prior subjection of the cells to unrelated insults such as respiratory blockade. Third, the initial phase of depolarization, which consumed less – often much less – than 30% of the resting voltage, was associated with a clear decrease of membrane resistance, thus permitting calculation of the actual influx of cationic charges.

Simple maintenance of bulk cytoplasmic electroneutrality during the influx of LSI charges requires balancing charge movements: some combination of efflux of cytoplasmic cations and influx of extracellular anions. The resting membrane voltage of *Neurospora* (and presumably also of *Saccharomyces*) is sustained predominantly by a pumped efflux of protons, which are largely recycled via cotransporters to fuel the uptake of nutrients [2–6]. TPP^+ or TPA^+ current should replace some of the recycled protons (and, of course, short-circuit some of the nutrient porters), thereby revealing an increased net proton efflux.

The first objective, then, of the experiments described below was to determine the predicted H^+ efflux. Careful measurements under a variety of conditions, however, found a significant proton efflux associated with TPP^+ or TPA^+ uptake by *Neurospora* only at the lowest useful concentrations (1–2 mM), and instead, revealed an apparent proton *influx* at higher concentrations. The results implied that other ion movements must also occur and led to a detailed study of the behavior of Na^+ and K^+ in response to several different lipid-soluble cations. Substantial effluxes of these ions were indeed observed during LSI uptake, but were considerably smaller than the measured influxes, thereby implicating still other, unidentified, ion movements. The ensemble of results indicates that the processes by which TPP^+ and TPA^+ (and probably other small lipid-soluble cations as well) enter walled eukaryotic cells are predominantly electroneutral.

2. Materials and methods

2.1. Strains and methods for growth

Strains, and methods for growth and handling of cells are given in the previous paper [1], along with the relevant ancillary techniques for measurement and calculation. Chemical fluxes from millimolar extracellular concentrations of LSI's could not be assayed via extracellular ion-specific electrodes, so conventional chemical flux experiments were used to determine the uptake of tritiated TPP^+, as well as the concomitant release of intracellular K^+, Na^+, and H^+.

2.2. Chemical flux measurements

For determination of LSI, K^+, and Na^+ fluxes, cells of *Neurospora* grown 9–13 h in shaking culture (25°C) were suspended at densities of 2–4 mg (dry weight) per ml in 35 ml of flux buffer and equilibrated at 25°C for 30 min, on a water-bath shaker. Flux-buffer solutions, which were those listed in Table 1 of the previous paper [1], have been specifically cited here in each figure legend. After a 5-ml aliquot of the suspension was withdrawn for control assays, LSI dissolved at double strength in the appropriate buffer was diluted 1:1 into the cell suspension, and 8-ml samples were withdrawn for analysis at intervals of approximately 1 min, 3, 6, 10, 15, 25, 40, and 60 min. The samples were filtered through polycarbonate membranes (type PC, Nucleopore, Pleasanton CA), rinsed three times with 10 ml of distilled water, dried over calcium chloride at room temperature for 24 h, split, and weighed in two fragments.

Sodium and potassium contents were determined from the larger fragment (usually about 3/4 of the total pellet), following extraction in 1 M HCl (100°C, 1 h), by conventional flame photometry on an IL-143 photometer (Instrumentation Laboratories, Lexington, MA), using an internal lithium standard. TPP^+ and TPA^+ contents, labelled with tritiated derivatives (gift from Dr. H.R. Kaback, University of California at Los Angeles), were determined on the smaller fragment, which was extracted directly into scintillation fluid (Ready-Solv; Beckman Instruments, Fullerton, CA). ^3H was counted in a Beckman LS3150 scintillation counter. Cytoplasmic concentrations of K^+, Na^+, and TPP^+ were calculated from the ratio of total ion to dry weight by multiplying by 0.45. (This figure differs from the ratio, dry weight/intracellular water, previously used [1], in order to allow for the measured water content of pellets dried at room temperature [7].)

For determination of H^+ fluxes, 6- to 10-h shaking-culture cells were harvested, rinsed, and resuspended, as described above, in 15 ml of dilute buffer ($0.1 \times K \cdot$ DMG or $0.1 \times K \cdot$ Hepes; see Table 1, Ref. [1]) supplemented with KCl to contain 25 mM K^+. The suspension was shaken vigorously, poured into a water-jacketed vessel at 25°C, and stirred with a magnetic flea. The vessel was capped with a multiport stopper containing a sintered glass bubbler for aeration, a small pH electrode (Model V-708, Markson Science, Phoenix, AZ), plus a reference junction, syringe ports for injecting and withdrawing fluid, and an oxygen electrode (in some experiments; Model 5331, Yellow Springs Instrument, Yellow Springs, OH) to verify that the cell suspensions remained oxygenated. After a 5-min preincubation, allowed for stabilizing temperature and oxygen concentration and for determining the baseline rate of proton release, LSI (from 60 mM stock solu-

tions in the test buffer) was injected to a final concentration of 2, 7, or 20 mM. An injection transient lasting several sec always occurred with this procedure, even when solution in the vessel contained buffer *without* cells. Therefore each experiment was compared with a buffer control. Solution pH, recorded on a strip-chart recorder (Model BD11-744E, Kipp and Zonen, Delft, The Netherlands), was followed for 3–10 min after the LSI injection, and the differential slope was used to calculate apparent H^+ fluxes. At the end of each run, cells were reharvested, rinsed, dried, and weighed, as described above.

2.3. Computations

Strip-chart data were digitized on a BitPad S2 (SummaGraphics, Norwalk, CT). All flux data and summary results throughout were fitted to empirical equations (see text and figure legends) by means of the Marquardt algorithm [8] for non-linear least-squares. Multicompartment flux equations, Eqs. (3)–(5), for modelling TPP^+-uptake data (Figs. 6–9) were modified slightly from ones published previously [9]. Model computations were carried out with MathCAD software (MathSoft, Cambridge, MA). Display graphics for all figures were created via a program written by Dr. Bliss Forbush, III (Yale Department of Cellular and Molecular Physiology). Cellular ion concentrations are stated as 'mM', which means mmol/kg cell water.

3. Results

3.1. LSI-induced proton efflux

Initial attempts to measure extracellular acidification upon addition of higher concentrations of TPP^+ or TPA^+ to suspensions of *Neurospora* failed, but careful examination of pH records in response to additions of 1–2 mM LSI did reveal a brief net efflux from the cells. Digitized sample records, from an experiment with 2 mM TPP^+, are shown in Fig. 1. Accurate estimation of the cellular effects of added LSI's demanded correction for an injection artifact in the buffer alone (1st trace in Fig. 1). Correction was accomplished by digitizing both the experimental records (e.g., 2nd trace in Fig. 1) and each corresponding control record, superposing the two at the time of LSI addition, subtracting, and fitting the resultant difference curve (3rd trace, Fig. 1) segmentally: using a straight line for the preincubation period and a single decaying exponential (see lowest trace of Fig. 1) for the period 2–6 min following the LSI injection.

In the example shown, the increased acid release implied an apparent stimulation of proton efflux by 1 mM/min. Averaged results from all experiments con-

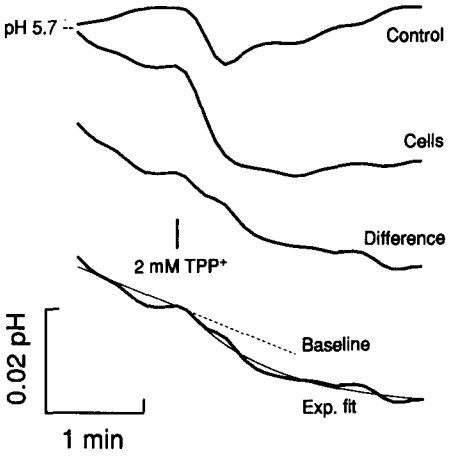

Fig. 1. Small proton efflux associated with TPP^+ uptake by *Neurospora*. Curves (top to bottom): 1st, buffer alone; 2nd, buffer + cells; 3rd, 2nd minus 1st; 4th, analysis of 3rd. Cells suspended at 2 mg dry wt/ml in 0.1×K·DMG buffer (see Table 1, Ref. [1]) supplemented to 25 mM K^+ with KCl, and vigorously aerated. 2 mM TPP^+ injected as indicated. Strip-chart records digitized on a BitPad 2 (see Materials and methods). Baseline: linear regression to the whole pre-TPP^+ period, with fitted slope = −0.012 pH/min, ≈ steady release of 0.6 mM H^+/min, referred to intracellular water. Exp. fit: to data post-TPP^+ injection, with rate constant of 1.07/min and a span of 0.021 pH, giving an initial rate = −0.023 pH/min. Initial slope difference: 0.011 pH/min ≈ 0.85 mM H^+/min. Data from a representative experiment (1 of 5) with 2 mM TPP^+.

ducted under this condition ($n = 5$; pH 5.6, 1 mM Ca^{2+}) are plotted in Fig. 2A and yielded an apparent proton efflux slightly greater than 3 mM/min. This flux is commensurate, as will be shown in the next section (Figs. 5,8), with the actual influx of lipid-soluble ions observed under comparable conditions, i.e., 2 mM TPA^+ in the presence of 1 mM extracellular Ca^{2+}. It is also commensurate with the current which would be expected from electrical measurements (Fig. 8 and related text, Ref. [1]), if current induced by TPP^+ were proportional to the extracellular concentration of that ion. (As has already been noted [1], whole-cell electrical records were too noisy to yield reliable current and resistance measurements in response to 1–2 mM TPP^+.)

Thus, we cannot rule out the possibility that *initial entry of* TPP^+, at extracellular concentrations near or below 2 mM, represented electrophoretic entry: driven by the membrane voltage, and exchanging extracellular LSI's for outwardly pumped protons. But that uncomplicated process – if indeed it does occur – is brief, at most a few minutes for low concentrations and much less for high concentrations, and does not allow the LSI's to equilibrate with membrane voltage [1].

Many observations suggest, however, that the similarity in magnitude of the apparent H^+ efflux, on the one hand, and the measured influx of LSI's or estimated inward current, on the other hand, is coincidental rather than causal. The most immediate such obser-

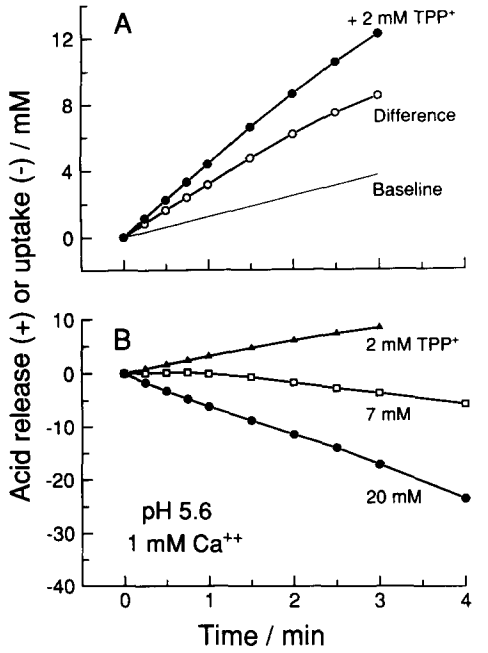

Fig. 2. Summary of apparent H^+ movements stimulated by extracellular TPP^+. (A) Averaged results for five experiments like that of Fig. 1, but with ΔpH vs. time converted to apparent $\Delta[H^+]$ vs. time. (B) Averaged $[H^+]$ effects of TPP^+ at three different concentrations. Curve for 2 mM TPP^+ (▲) is rescaled from the *difference* curve (○) in the top panel. 0.1×K·DMG buffer containing 1 mM $CaCl_2$. Net *efflux* of protons was observed only at the lowest TPP^+ concentration.

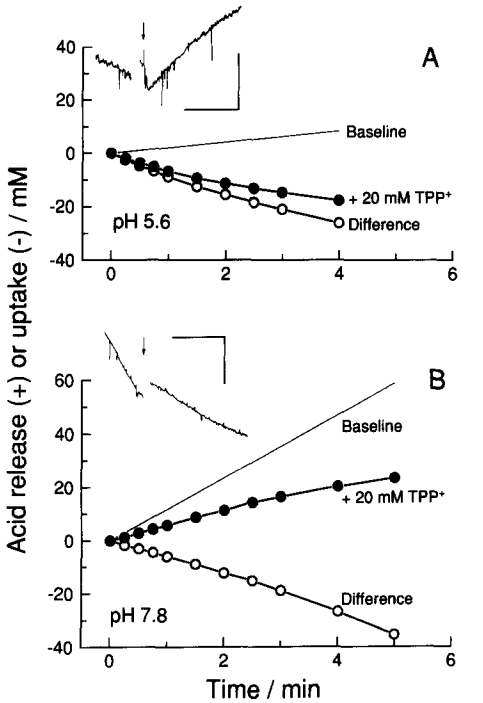

Fig. 3. Apparent proton *influxes* induced by 20 mM TPP^+. (A) pH 5.6; cells incubated in 0.1×K·DMG buffer without Ca^{2+}; TPP^+ injected at zero time. Average of three experiments. Baseline H^+ release: 2.18 mM/min. (Inset) Trace of pH_o during one of the three experiments, showing actual alkalinization of the medium. Scale bars, 2 min, 0.2 pH. (B) pH 7.8; cells incubated in 0.1×K·Hepes buffer with 1 mM $CaCl_2$. Average of four experiments. Baseline H^+ release: 11.86 mM/min. (Inset) Trace from one experiment, showing the apparent proton influx as a reduction from steep baseline H^+ release. Scale bars: 2 min, 0.1 pH.

vations are that neither extracellular pH nor the presence/absence of Ca^{2+}, nor elevation of extracellular LSI (above 2 mM) altered the apparent proton efflux in an appropriate fashion. As is seen in Table 1, the presence or absence of millimolar extracellular calcium had no effect on the apparent proton fluxes, except perhaps for the low pH at 7 mM TPP^+. Extracellular pH, likewise, had little effect, again with exception of a single comparison: 5.6/7.8 for the lowest TPP^+ concentration (2 mM). Finally, under almost all conditions – that is, at high pH, or with $[TPP^+] \geq 7$ mM, and with or without Ca^{2+} – the induced apparent flux of protons was either zero or negative (inward). Averaged plots for all three TPP^+ concentrations tested at pH 5.6 with 1 mM Ca^{2+}, are shown in Fig. 2B, and Table 1 summarizes the total results. These effects on H^+ efflux contrast in most particulars with the effects of the same agents on influxes of LSI's (documented later, in Figs. 5–9): there, elevating extracellular pH and/or LSI concentration unequivocally increased the flux, and adding millimolar Ca^{2+} diminished the flux.

Table 1
Apparent initial proton fluxes[a] induced by LSI

pH_o	$[Ca^{2+}]_o$	External TPP^+ concn.		
		2 mM	7 mM	20 mM
5.6	0	+2.3	−8.0	−10.0
	1 mM	+3.2	+0.3	−6.3
7.8	0	−1.1	−0.6	−6.8
	1 mM	–	−0.3	−5.6

[a] Reported as mmol/kg cell water per min (mM/min), with + meaning efflux, and − meaning influx. Averages for 2–5 experiments. Average baseline H^+ efflux: at pH 5.6 2–3 mM/min, at pH 7.8 8–12 mM/min.

The observation of net proton influx (or alkali efflux) accompanying uptake of TPP^+ or TPA^+ is documented in Fig. 3A for an experiment at low pH, and in Fig. 3B at high pH. In the latter case, the calculated influx represented a reduction from the very steep baseline acidification (proton efflux), whereas in the former case frank alkalinization occurred, i.e., the pH of the medium actually rose steadily after addition of 20 mM TPP^+ to the cell suspension. This was evident in all individual records made at pH 5.6–5.8, as well as in the summary plots. Thus, the LSI-induced proton influx could not be attributed simply to metabolic blockade, since – as is demonstrated in Fig. 4 – that led to a reduction of proton efflux but not to net proton influx, either at high pH (Fig. 4A) or low pH (Fig. 4B). In fact, for *Neurospora*, which is an obligate aerobe, mitochondrial blockade per se was shown in

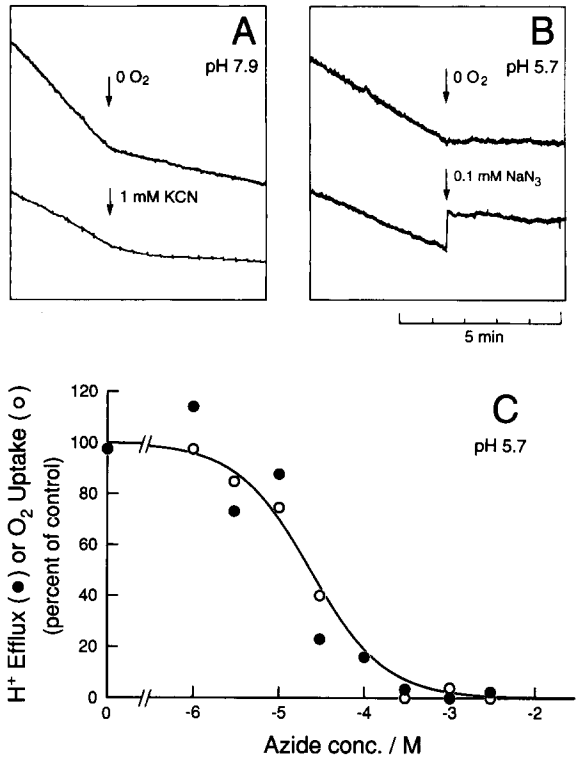

Fig. 4. Demonstration of the *absence* of proton influx during simple respiratory blockade of *Neurospora*. (A) pH_o records at pH 7.9, to show effects of anoxia and of 1 mM cyanide; buffer: 0.2×K·Hepes with 1 mM $CaCl_2$. Calibration = baseline H^+ release: 33.5 mM/min at 30°C (top), and 14.0 mM/min at 25°C (bottom). (B) pH_o records at pH 5.7, showing effects of anoxia and azide; buffer: 0.2×K·DMG with 1 mM $CaCl_2$; 20°C. Calibration = baseline H^+ release: 7.6 mM/min (top) and 5.6 mM/min (bottom). Note especially that none of these inhibitors, at either low or high pH, induces net proton influx. (C) Parallel shifts of net proton release (●) and oxygen consumption (○), as revealed by a dose-response plot for sodium azide. Sequence of nine trials similar to that in panel B (bottom trace); 25°C. Smooth curve is for single-site titration, with a least-squares pK_d of 4.6.

separate experiments (Fig. 4C) to produce a parallel *decline* in respiration and in the rate of medium acidification; it never produced alkalinization of the medium. (This statement holds during normal carbon and nitrogen metabolism; *Neurospora* utilizing nitrate as the sole nitrogen source does show baseline alkalinization (Slayman, C.L., unpublished experiments), as is also true in many plant species [10,11].) It should be emphasized, again, that the magnitude of LSI-induced proton influx (or alkali efflux) was independent of extracellular pH and calcium concentration.

3.2. Uptake of lipid-soluble cations

As was demonstrated in the previous paper [1], net uptake of LSI's from micromolar concentrations was rapid but brief, a quasi steady-state being reached within 1–2 min for both *Neurospora* and *Saccharomyces*. In the case of *Neurospora*, the initial influx from 100 μM extracellular TPP^+ was ~ 14 mM/min, with a half-time of ~ 8.5 s. A small slow entry process was also discernable in those data (Fig. 4, Ref. [1]), roughly linear in time, at < 0.1 mM/min.

Uptake from millimolar LSI concentrations proved much more prolonged, but it too displayed two components: an initial influx having an (exponential) rate constant of about 1 min^{-1}, plus a quasi-linear component which could last an hour or more and was strongly inhibited by millimolar calcium. Results for uptake of TPP^+ and TPA^+ from media at pH 5.8 are summarized in Fig. 5. Empirically, all such uptake curves could be described by an equation of the form

$$C_i = a(1 - e^{-\alpha t}) + d \cdot t \quad (1)$$

and all of the data in Fig. 5 could be fitted with a single α, whose least-squares value was 0.907 min^{-1}. The six values for a and d are listed in the legend table to Fig. 5. While calcium essentially blocked the slow component of LSI entry, it had only a minor depressing effect on the fast component (except perhaps at the lowest LSI concentration).

Considering normal cell structure, two-component loading curves like those in Fig. 5 are most easily related to a three-compartment model for TPP^+ trans-

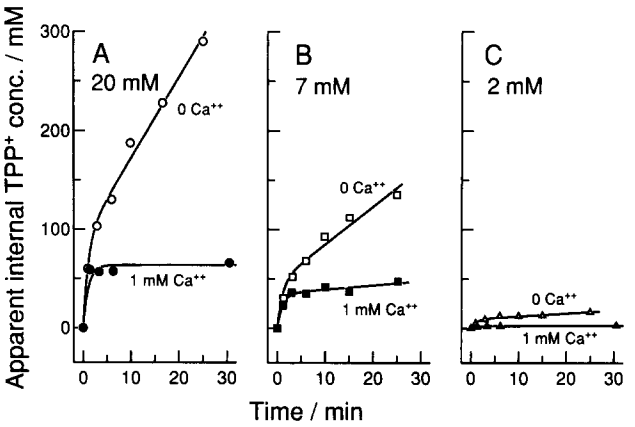

Fig. 5. Kinetics of the uptake of lipid-soluble ions by *Neurospora*: Part I. Concentration dependence, and the suppressing effect of extracellular calcium; pH 5.8. Cells preincubated in Na·DMG with (●,■,▲) or without (○,□,△) 1 mM $CaCl_2$. 2, 7, or 20 mM ^{3}H-TPP^+ (or 30 mM ^{3}H-TPA^+) added at zero time. Curves fitted by two-component kinetics, with an exponential initial component plus a steady linear component (text Eq. (1)): $a \cdot \exp(-\alpha \cdot t) + d \cdot t$. Flux parameters:

	$[TPP^+]_o$	$[Ca^{2+}]_o$	a (mM)	α (1/min)	d (mM/min)
A	20 mM	0	89.9	0.907	8.20
	30 mM [a]	1.0 mM	63.6	↓	0.04
B	7 mM	0	46.4		3.83
	7 mM	1.0 mM	34.8		0.42
C	2 mM	0	9.09		0.30
	2 mM [a]	1.0 mM	2.32		0.02

[a] ^{3}H-TPA^+ used instead of ^{3}H-TPP^+ for these two curves.

fer, in which the isotopically labelled ion moves first from the extracellular solution (O) into the bulk or 'free' cytosol (C), and then to an internal storage compartment (S) whence it has no direct access to the plasma membrane. This simple arrangement is represented as the main part of a more complicated diagram, in Fig. 6A. It proved adequate for analyzing all of the LSI-uptake curves at pH 5.8 and most at pH 8.2 (see Fig. 8, below).

Solution of the first-order rate equations for a three-compartment series model (right 3/4 of Fig. 6A, with $k_{op} = k_{po} = 0$) is simplified by equating the apparent linear component in Fig. 5 with a large, slow exponential, so that the fitting equation becomes

$$C_i = a(1 - e^{-\alpha t}) + b(1 - e^{-\beta t}) \quad (2)$$

Comparing the derivatives of Eqs. (1) and (2), when $t = 0$, $d = b\beta$, and a lower bound can be placed on β by first estimating the maximal deviation from linearity which could be masked by scatter of data, in the uptake plots shown. From trial calculations at the end of the measuring period (25 min), no more than 10% deviation could be masked in any of the TPP^+-uptake curves. That leads to a rough lower bound of 0.01 on β, so $b \approx d/\beta$ can be calculated. The resultant values are surprisingly large, several hundred millimolar (for $[TPP]_o \geq 7$ mM) at pH 5.8 in the absence of calcium. (The *physical* significance of these large values is unclear; the important parameter in the measurements, of course, is $b\beta$.) By using the facts (i) that $[TPP^+]_c = [TPP^+]_s = 0$ at zero time, and (ii) that the outside compartment (O) is large enough to keep $[TPP^+]_o$ fixed at the starting value, the model rate constants and compartment sizes (Fig. 6A) can be written as

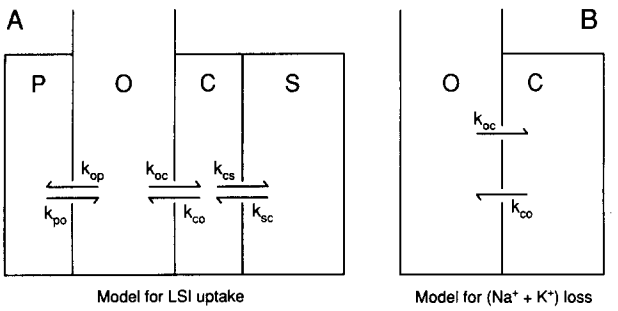

Fig. 6. Diagrams of compartmental flux models. (A) Bifurcated 4-compartment model for TPP^+-uptake data of Figs. 5 and 8. O, outside; C, bulk cytosol; S, internal subcompartment (vacuoles?). These three compartments are assumed to be functionally in series in all LSI transport experiments. P, parallel extracellular compartment (cell wall?); only the data for high pH at the highest LSI concentration (≥ 20 mM) demand this compartment. (B) Two-compartment model for the $\{Na^+ + K^+\}$-loss data of Figs. 10–12. Those data do not require either S or P compartments. Arrows and k values designate first-order rate constants for flux in the direction indicated.

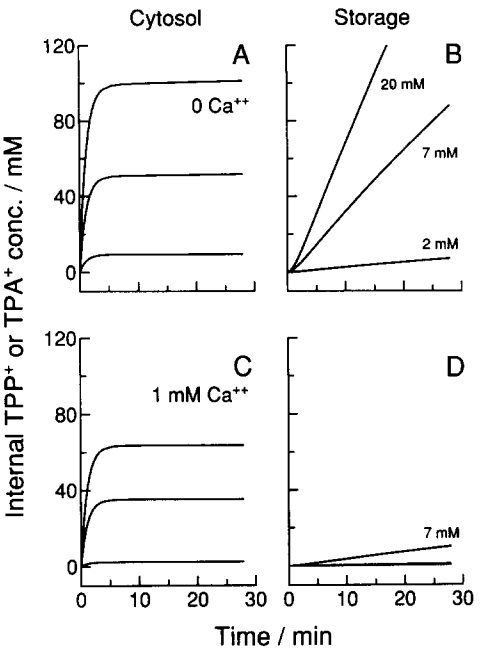

Fig. 7. Quantitative analysis of TPP^+ uptake by *Neurospora* at pH 5.8: filling of cytoplasmic (A,C) and storage (B,D) compartments in the absence (A,B) and presence (C,D) of 1 mM $CaCl_2$. Fitted parameters in Fig. 5 used to calculate model parameters in Fig. 6A (3-compartment series arrangement), via text Eqs. (3)–(5). To simplify the series compartment analysis, the linear component in Fig. 5 was equated to a large slow exponential component, with a pseudo-rate constant of 0.01 min^{-1} (see rationale in text). Compartmental parameters:

Conditions $[LSI]_o$	Fast compart. (C)			Slow compart. (S)		
	k_{oc} (1/min)	k_{co} (1/min)	C_c (mM)	k_{cs} (1/min)	k_{sc} (1/min)	C_s (mM)
0 Ca^{2+}						
20 mM	4.49	0.825	109	0.081	0.011	801
7 mM	6.56	0.832	55.2	0.074	0.011	374
2 mM	4.27	0.875	9.76	0.031	0.010	29.3
1 mM Ca^{2+}						
30 mM [a]	1.92	0.897	63.6	0.001	0.010	3.68
7 mM	4.57	0.895	35.7	0.012	0.010	41.5
2 mM [a]	1.06	0.899	2.36	0.007	0.010	1.71

[a] ^3H-TPA^+ used instead of ^3H-TPP^+ for these two curves.

follows, in terms of the empirical compartment sizes (a, b) and rate constants (α, β):

$$k_{oc} = \frac{a\alpha + b\beta}{C_o}, \quad k_{co} = \frac{a\alpha^2 + b\beta^2}{k_{oc}C_o} \quad (3a,b)$$

$$k_{cs} = \alpha\beta\left[\frac{a+b}{k_{oc}C_o} - \frac{1}{k_{co}}\right], \quad k_{sc} = \frac{\alpha\beta}{k_{co}} \quad (4a,b)$$

$$C_{c\infty} = \frac{k_{oc}}{k_{co}}C_o, \quad C_{s\infty} = \frac{k_{cs}}{k_{sc}}C_{c\infty} \quad (5a,b)$$

in which C_o, $C_{c\infty}$, and $C_{s\infty}$ are the end values of $[TPP^+]$ in the outside, cytosolic, and internal storage compartments, respectively [9].

Application of this analysis to the fitted curves of Figs. 5 yielded the compartmental behavior shown in Fig. 7. The results provide a quantitative description of the concentration dependence of LSI entry into both compartments, as well as of the selective inhibitory effects of extracellular free Ca^{2+}. The efflux rate constants for both compartments (k_{sc} and k_{co}) were insensitive to concentration and to calcium. The calculated influx rate constants (k_{oc} and k_{cs}) were more variable than might have been expected as functions of LSI concentration, but were clearly reduced by millimolar free Ca^{2+}, the reduction factor being 1.5- to 4-fold for flux (k_{oc}) from outside to cytosol, and about 5- to > 50-fold for flux (k_{cs}) from cytosol to the postulated storage compartment. The apparent stable cytosolic concentrations ($C_{c\infty}$) were reduced about 2-fold by 1 mM $[Ca^{2+}]_o$, and the calculated saturating storage concentrations ($C_{s\infty}$) were reduced 9- to > 200-fold.

In the experiments at pH 5.8, the three-compartment analysis above yielded steady concentration ratios ($C_{c\infty}/C_o$) which – for all TPP^+ and TPA^+ concentrations – either were less than the calculated equilibrium distributions, given residual membrane voltage (V_m) as described previously [1], or were not sufficiently greater to warrant more elaborate calculations.

The same was true, as well, for most experiments at higher pH, but at the highest LSI concentrations tested at pH 8.2 (also the highest pH tested), another phe-

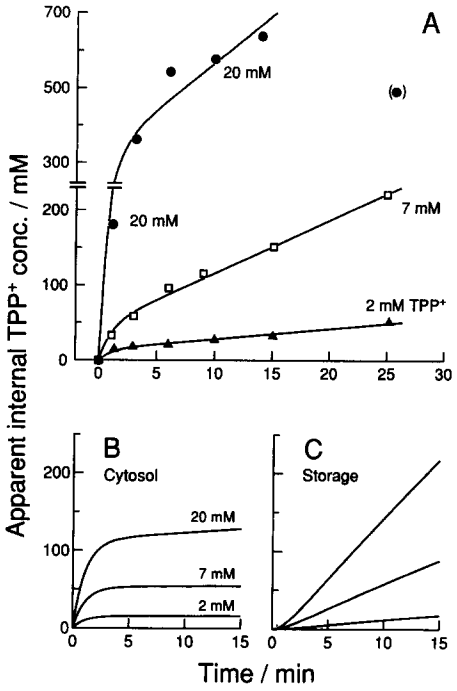

Fig. 8. Kinetics of the uptake of lipid-soluble ions by *Neurospora*: Part II. Concentration dependence at high pH (8.2). Companion experiment to that of Fig. 5; cells preincubated in Na · Hepes buffer without calcium. (A) Data, with curves fitted via text Eq. (1). Note scale change midway along the ordinate. Rate constant (α) for the fast component held in common for these fits and those of Fig. 5. Fitted flux parameters:

$[TPP^+]_o$	a (mM)	α (1/min)	d (mM/min)
20 mM	322	0.907	24.7
7 mM	45.4	↓	7.08
2 mM	14.2		1.40

(B and C) Quantitative analysis of fluxes, via text Eqs. (3)–(5). Series compartment calculation similar to that used in Fig. 7, but augmented for 20 mM TPP^+ by assigning excess 'cytoplasmic' TPP^+ to a parallel extracellular compartment: P, in the diagram of Fig. 6. That is, the extrapolated end value of $[TPP^+]_c$ was limited by presumed equilibration with the plasma membrane voltage (see Fig. 9 of Ref. [1]). Calculated compartmental parameters:

$[TPP^+]_o$	Fast compart. (C)			Slow compart. (S)			Parallel comp. (P)		
	k_{oc} (1/min)	k_{co} (1/min)	C_c (mM)	k_{cs} (1/min)	k_{sc} (1/min)	C_s (mM)	k_{op} (1/min)	k_{po} (1/min)	C_p (mM)
20 mM	8.34	0.774	157	0.131	0.012	2414	7.10	0.907	212
7 mM	6.90	0.775	62.3	0.130	0.012	691	–	–	–
2 mM	7.13	0.819	17.4	0.087	0.011	136	–	–	–

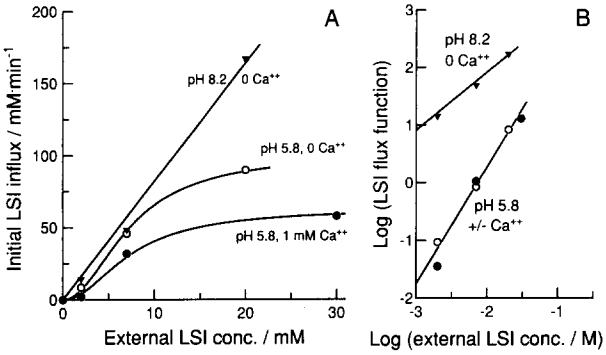

Fig. 9. Concentration dependence of initial cytosolic influxes of TPP^+. (A) Cartesian plot of influx versus extracellular concentration, showing the pronounced sigmoid shape at pH 5.8, and near linearity at pH 8.2. (B) Hill plots of the same results. Initial slopes were measured in Figs. 7A, 7C, and 8B, and were found equal to the calculated initial slopes, $J_{oc} = k_{oc}C_o$, from the corresponding compartmental parameters (see legends to Figs. 7 and 8). The 'flux function' indicated on the ordinate scale for the Hill plots is simply the flux J_{oc} for results at pH 8.2, and is the ratio $J_{oc}/(J_{max} - J_{oc})$ for the results at pH 5.8. A straight line, $J_{oc} = k_{oc}C_o$, was used to fit the pH-8.2 plot in panel A, and text Eq. (6), $J_{oc} = J_{max}C_o^n/(K_{0.5}^n + C_o^n)$, to fit the pH-5.8 plot, yielding the following least-squares parameters: $k_{oc} = 8.18\ min^{-1}$, $J_{max}(0\ Ca^{2+}) = 101$ mM/min, $J_{max}(1$ mM $Ca^{2+}) = 62.2$ mM/min, $K_{0.5} = 7.54$ mM, and $n = 2.02$.

nomenon appeared. Plots of TPP^+ uptake data at pH 8.2 are shown in Fig. 8A, and the corresponding analysis is summarized in Figs. 8B, 8C. After several minutes of exposure to 20 mM TPP^+, $[TPP^+]_c$ – calculated in simple fashion from Eqs. (3)–(5) – appreciably exceeded the equilibrium concentration expected from the residual V_m [1]. In order to rationalize this observation, an additional extracellular compartment was postulated (diagrammed as P in Fig. 6A), existing under this special condition kinetically in parallel with the cytosol and loading at the same empirical rate. Then the stable end concentration of cytosolic TPP^+ ($C_{c\infty} = [TPP^+]_{c\infty}$) was assumed to be limited by V_m, with excess TPP^+ lodging in the parallel extracellular compartment. The resultant cytosolic uptake curve, and the simpler ones for the smaller values of $[TPP^+]_o$ are compared in Fig. 8B. The ensemble closely resembles the curves for pH 5.8, so that extracellular pH, per se, did not much affect LSI entry across the plasma membrane. Evidently the high pH did, however, enhance by ~2-fold sequestration of LSI into the series intracellular compartment (Fig. 8C).

Finally, comparison of the overall results at pH 5.8 and 8.2 revealed a pH-dependent shift in the apparent kinetic order of TPP^+ influx (Fig. 9). At pH 8.2, the initial influx, J_{oc} – whether measured from the plots of Fig. 8A or calculated from the model parameters ($= k_{oc}C_o$) – was nearly linearly related to extracellular concentration. But at pH 5.8 that was clearly not the case, and as shown in Fig. 9A, the influx curve was sigmoid and appeared to saturate with rising extracellular concentration. This concentration dependence could easily be described (see Fig. 9B) by a simple Hill equation,

$$J_{oc} = \frac{J_{max}(C_o)^n}{(K_{0.5})^n + (C_o)^n} \quad (6)$$

in which J_{max} and $K_{0.5}$ are the usual 'Michaelis' parameters, and n (the Hill coefficient) is the cooperativity factor, which in this case gave a least-squares value (2.02) not significantly different from 2.

3.3. Description of LSI-induced cation release

Since the measured proton fluxes associated with the uptake of lipid-soluble cations did not approach charge balance, even in direction for most experiments, it was clear that other ion fluxes must occur. The only other ions available for counter-flux charge balance, and likely to be present in sufficient quantity, are the major cytoplasmic alkali-metal cations, Na^+ and K^+. And the background literature on both *Saccharomyces* [12–14] and *Neurospora* [3,9] indicated these ions to be likely candidates for exchange with LSI's, because they do in fact efflux during uptake of a variety of *amino* cations. In the present experiments, displacements of Na^+ and K^+ were examined separately, on appropriately preloaded *Neurospora*, in response to TPP^+, TPA^+, and a third analogue, triphenylmethylphosphonium ion ($TPMP^+$). Although the displacement of Na^+ and K^+ by each other is very asymmetric [7,15] – micromolar K^+ being sufficient to displace millimolar Na^+ (especially in the presence of extracellular Ca^{2+}; Slayman, C.L., unpublished experiments), quantitative discrimination between the two species was small with respect to LSI effects.

(Throughout the discussion below, the total cellular concentration of sodium + potassium ($[Na^+ + K^+]_c$) is reported, since this gave much less scattered results than the separate values of $[Na^+]_o$ or $[K^+]_o$. In the usual high-K^+ cells, ~90% of the sum is potassium; while in K^+-depleted, Na^+-loaded cells, ~80% of the sum is sodium. For *Neurospora* the absolute value of $[Na^+ + K^+]_c$ ranges from 160 to 200 mM [6,7,16] in the normal growth media, and 180 mM was taken here for normalizing data from different experiments.)

The extent of LSI-stimulated release of $\{Na^+ + K^+\}$ from *Neurospora* varied greatly with conditions, but one overriding observation was clear: in the presence of extracellular calcium (1 mM), alkali cation loss from the cells was slow and monophasic, whereas in the absence of extracellular calcium the loss was rapid and diphasic. Extracellular pH also had pronounced effects on the effluxes.

All efflux curves could be fitted as the sum of two exponential processes in time, similar to Eq. (2), but declining rather than rising, so

$$C_i = ae^{-\alpha t} + be^{-\beta t} + c \quad (7)$$

where C_i is the total cytosolic concentration, $[Na^+ + K^+]_c$. For the homogeneous set of experiments shown in Figs. 10–12 below, all curves drawn were fitted to the plotted data with the rate constants α and β adjusted in common for all 15 plots and having least-squares values of 0.967 min^{-1} and 0.133 min^{-1}, respectively.

The results shown in Fig. 10 (parts A and B) are directly comparable with those of Fig. 5 (0 Ca^{2+}) and Fig. 8 on TPP^+ uptake, since the data were obtained

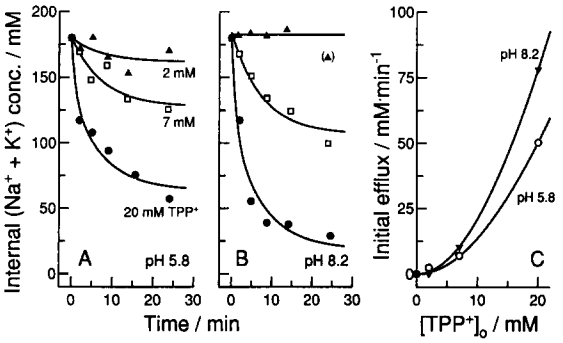

Fig. 10. Kinetics of alkali-metal cation efflux from *Neurospora*, induced by lipid-soluble ions. Part I: Dependence on $[TPP^+]_o$ and pH_o. (A) At pH 5.8. Cells incubated in Na·DMG buffer without Ca^{2+}. (B) At pH 8.2. Cells incubated in Na·Hepes buffer without Ca^{2+}. For an empirical description, all curves were fitted by text Eq. (7), $a \cdot \exp(-\alpha t) + b \cdot \exp(-\beta t) + c$, but only a single component was required for the data at 2 and 7 mM, whereas two components were required at 20 mM. Rate constants fitted in common for all curves in Figs. 10, 11, and 12. Zero-time points are for cell samples harvested 1–4 min prior to injection of the LSI's. Bracketed point (▲) not included in the fit. Data normalized to total $[Na^+ + K^+]_c = 180$ mM at zero time, which is the generally established value for normal *Neurospora* [6,7,16]; actual values varied between 230 mM and 250 mM in these runs. Same experiments as in Figs. 5 and 8. Flux parameters:

$[TPP^+]_o$	a (mM)	α (1/min)	b (mM)	β (1/min)	c (mM)
A. pH 5.8					
20 mM	42.1	0.967	72.7	0.133	63.8
7 mM	0	↓	52.6	↓	127
2 mM	0		18.1		162
B. pH 8.2					
20 mM	67.8	0.967	95.5	0.133	18.7
7 mM	0	↓	77.3	↓	107
2 mM	0		0		183

(C) Initial effluxes in A and B, calculated as $-(\alpha a + \beta b)$ and plotted against extracellular $[TPP^+]$; for demonstration of cooperative effect and comparison with the TPP^+ influxes in Fig. 9. Curves fitted by least squares [8] for the Hill equation (text Eq. (6)), with the following parameters: apparent J_{max}(pH 5.8) = 540 mM/min; apparent J_{max}(pH 8.2) = 840 mM/min; apparent $K_{0.5}$ = 62.3 mM TPP^+; and n fixed at 2.0 (least-squares value = 2.15).

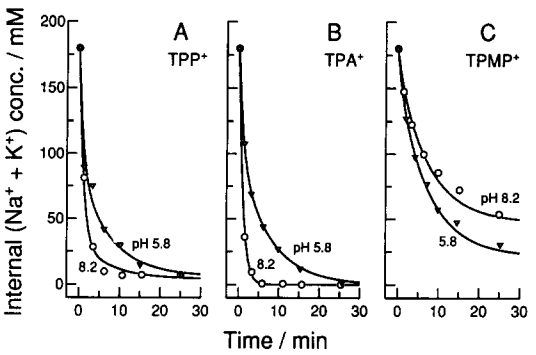

Fig. 11. Kinetics of LSI-induced loss of cellular cations. Part II: Comparison of high and low pH and of several LSI's at high concentration. (A) 20 mM TPP^+; (B) 30 mM TPA^+; (C) 30 mM $TPMP^+$. Cells incubated in K·DMG or Na·Hepes. General description of experiments, plus handling and fitting of the data were as in Fig. 10. Data normalized to total $[Na^+ + K^+]_c = 180$ mM at zero time; actual values varied between 140 mM and 160 mM. Fitted parameters:

LSI	pH_o	a (mM)	α (1/min)	b (mM)	β (1/min)	c (mM)
TPP^+	5.8	88.3	0.967	81.6	0.133	6.25
	8.2	149	↓	28.6	↓	4.00
TPA^+	5.8	80.5		100		0
	8.2	179		0		0
$TPMP^+$	5.8	23.4		135		21.7
	8.2	11.5		120		47.5

simultaneously from the same cells. Apart from some data scatter, typical for high-Na^+ cells, the plots show clearly that cation loss differed from TPP^+ uptake in having a *non-linear* slow component. Probably coincidentally, the rate constant for the fast-phase efflux, 0.967 min^{-1}, was close to that (0.907) for LSI uptake. Fig. 10C shows also the initial efflux of $\{Na^+ + K^+\}$ plotted as a function of extracellular TPP^+ concentration. Again, the relationship was cooperative, and when fitted with the Hill equation (Eq. (6)) the plots gave a least-squares value of $n = 2.15$ for the cooperativity factor. Although the absolutes rates of cation loss at pH 8.2 were larger than those at pH 5.8, cooperativity was unmistakable at both pH values tested, thus differing clearly from TPP^+ influx. Furthermore – and again differing from the TPP^+ influx results – the efflux data showed no signs of saturation at the highest practicable LSI concentrations. (The calculated values of J_{max} and $K_{0.5}$ (see legend to Fig. 10), therefore, must be taken as computational conveniences rather than as serious parameter estimates.)

Surprisingly, TPP^+ and TPA^+ released cations from normal high-K^+ cells somewhat more rapidly and completely than from high-Na^+ cells, and also evinced a clearer kinetic distinction between pH 5.8 and pH 8.2 for the high-K^+ cells. Efflux curves elicited by the two LSI's, at both pH values, are shown in Fig. 11, along with corresponding curves produced by $TPMP^+$. The pH effect was clearest for TPA^+ (Fig. 11B): only the

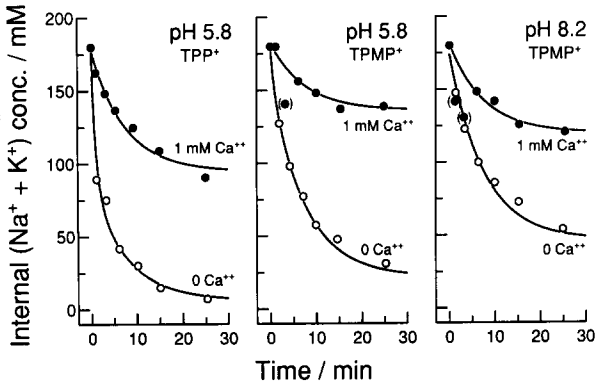

Fig. 12. LSI-induced loss of cellular cations. Part III: Effect of calcium. Cells incubated in K·DMG buffer With or without 1 mM $CaCl_2$; tested with 20 mM TPP^+, or 30 mM TPA^+ and $TPMP^+$. General description as in Figs. 10 and 11. Bracketed points (•) not included in the fits. Data normalized to total $[Na^+ + K^+]_c = 180$ mM at zero time; actual values varied between 150 mM and 180 mM. The two pH-5.8 curves for zero Ca^{2+} are reproduced from Fig. 11. Fitted parameters:

Ca^{2+} (1 mM)	a (mM)	α (1/min)	b (mM)	β (1/min)	c (mM)
pH 5.8, TPP^+					
Yes	0	0.967	83.2	0.133	94.4
No	88.3	↓	81.6	↓	6.25
pH 5.8, $TPMP^+$					
Yes	0		46.6		136
No	23.4		135		21.7
pH 8.2, $TPMP^+$					
Yes	0		61.7		120
No	11.5		120		47.5

single fast component of efflux was evident at pH 8.2, but the two components were of about equal size at pH 5.8. Results for TPP^+ were similar, but less extreme; and for $TPMP^+$ might be considered anomalous: the fast component of efflux was very small, and changing pH had no significant effect on efflux *kinetics* (as distinct from scale, or amplitude).

Finally, the effect of extracellular free Ca^{2+} on some of the LSI-induced cation effluxes is demonstrated in Fig. 12. Allowing for some scatter of data (bracketed points not included in the fits), extracellular calcium clearly eliminated the fast component of efflux, and reduced the slow component. This result makes an unequivocal separation between the kinetics of LSI uptake (Fig. 5) and the induced efflux of $\{Na^+ + K^+\}$, since in the former case calcium blocked the *slow* component but had relatively little effect on the fast component.

3.4. Quantitative modelling of LSI-induced cation efflux

Other aspects of the data also indicate that the two phases of cation efflux from *Neurospora* should not be identified with anatomical compartments in the manner implied by the analysis of LSI influx. Among these is the conspicuous fact that either fast efflux or slow efflux could encompass all, or almost all, of the total cation release (cf. Fig. 11B with 11C).

An alternative way of looking at the $\{Na^+ + K^+\}$-efflux data, then, is that all effluxing ions issue from the same anatomical compartment, but that the different treatments differentially affect the uptake and release processes responsible for steady-state maintenance of $[Na^+ + K^+]_c$. In other words, different LSI regimens, pH, and Ca^{2+} have different relative effects on the active and passive transport processes which determine steady-state cytoplasmic cation levels. The consequent imbalance would lead to net efflux of cytoplasmic cations, without any direct coupling to LSI entry. In its simplest form, this idea is an ensemble version of the accepted 'pump-leak' model of membrane transport, in which all significant uptake processes for K^+ and Na^+ are lumped together, and all release processes are likewise lumped together. The notion can be modelled very simply via the diagram of Fig. 6B, in which a single pseudo first-order reaction (k_{oc}) is presumed to dominate normal influx of cations from the medium to the cytosol, and another pseudo first-order reaction dominates efflux (k_{co}). Two-component efflux kinetics are generated, then, by supposing that LSI treatment has both an *immediate* effect on the rate constants, and a *delayed* effect. Evidence for one kind of delayed effect has already been presented, in connection with insult-induced decreases of membrane permeability [1], and for these efflux measurements, too, the delayed effect appears as a decrease in the flux constant.

An outline derivation of mathematical relationships for the specific model used here is given in the Appendix. The key equation is

$$C_c = \left(C_{cs} - \frac{k_{oc}}{k_{co}} C_o\right) e^{-k_{co}t} + \frac{k_{oc}}{k_{co}} C_o \qquad (8)$$

in which C_c and C_o have their previous meanings, C_{cs} is the starting value of C_c, and the rate constants k_{oc} and k_{co} are defined in Fig. 6B. This equations is a special solution to the differential equations for two-compartment flux, when the rate constants are fixed, and the external compartment is sufficiently large to hold C_o constant. We have applied it piecewise to the flux curves of Figs. 10–12, with three sets of rate 'constants', corresponding to 0) the pretreatment steady-state (k_{oc0}, k_{co0}); (1) the condition immediately induced by LSI's (k_{oc1}, k_{co1}); and – after an appropriate time delay (τ) – (2) the end steady-state representing cellular adaptation to LSI treatment (k_{oc2}, k_{co2}). Eq. (8) has several forms (Appendix Eqs. (A-3a–d)), because the value of C_{cs} changes from case (1) to case

(2), and because the appropriate time variable for case (2) is $(t-\tau)$.

Five of the six rate constants can be evaluated from the fitted parameters of Eq. (7), as follows:

$$k_{co0} = k_{co2} = \beta, \quad k_{co1} = \frac{\alpha a + \beta b}{a+b} \qquad (9a,b)$$

$$k_{oc0} = \frac{a+b+c}{C_o} k_{co0}, \quad k_{oc2} = \frac{c}{C_o} k_{co2} \qquad (9c,d)$$

while k_{oc1} and τ are adjusted to give best-fits of Eq. (8) to the empirical curves. The results of these calculations, for all 27 relevant LSI-induced cation efflux experiments, are summarized in Table 2. In all but three cases (the bracketed calculations for curves 10-1, 10-2, and 10-5), the curves obtained were superposable on the curves (e.g., Figs. 10–12) drawn by fitting Eq. (7) to the data. The initial cation effluxes, also listed in Table 2 (last column), were calculated directly from the empirical fits, as $J_{co0} = \alpha a + \beta b$.

Several significant comparisons can be extracted from Table 2 and the corresponding data plots (Figs. 10–12). Perhaps most importantly, effluxes of cytoplasmic cations induced by high concentrations of LSI's in the presence of millimolar Ca^{2+} were much too small (J_{co0} = 6–11 mM/min) to be the charge balance for

Table 2
Reaction parameters for the flux-relaxation model of LSI-induced cation release

Fig. No. [a] and curve	Lipid-soluble ion		pH_o	$[Ca^{2+}]$ (mM)	K^+/Na^+	C_{c0} [b] (mM)	$C_{c\infty}$ (mM)	τ (min)	k_{oc1} [c] (1/min)	k_{co1} (1/min)	k_{oc2} (1/min)	J_{co0} (mM/min)
	Type	mM										
10-1	TPP^+	2	5.8	–	Na^+	180	162	– [d]	0.855	0.133	0.855	2.40
								(–	0.965	0.149	0.965) [e]	
i	TPA^+	2	5.8	1	K^+	186	162	–	0.870	0.133	0.870	3.14
10-2	TPP^+	7	5.8	–	Na^+	180	128	–	0.676	0.133	0.676	6.97
								(–	0.965	0.181	0.965) [e]	
ii	TPP^+	7	5.8	1	K^+	193	152	–	0.801	0.133	0.801	3.43
10-3	TPP^+	20	5.8	–	Na^+	178	62.8	1.6	1.05	0.439	0.333	50.4
11-1	TPP^+	20	5.8	–	K^+	176	6.25	2.0	0.350	0.566	0.033	96.2
12-1	TPP^+	20	5.8	1	K^+	178	94.4	–	0.494	0.133	0.494	11.0
iii	TPP^+	20	5.8	1	Na^+	183	129	–	0.689	0.133	0.689	7.13
10-4	TPP^+	2	8.2	–	Na^+	183	183	–	–	–	–	0
iv	TPA^+	2	8.2	1	K^+	182	156	–	0.829	0.133	0.829	3.50
10-5	TPP^+	7	8.2	–	Na^+	184	107	–	0.572	0.133	0.572	10.3
								(–	0.965	0.204	0.965) [e]	
v	TPP^+	7	8.2	1	K^+	178	68.3	–	0.384	0.133	0.384	16.5
10-6	TPP^+	20	8.2	–	Na^+	182	18.7	2.7	0.961	0.479	0.099	78.3
vi	TPP^+	20	8.2	–	Na^+	180	24.7	3.5	1.07	0.854	0.131	133
11-2	TPP^+	20	8.2	–	K^+	182	3.99	3.5	0.500	0.833	0.212	148
11-3	TPA^+	30	5.8	–	K^+	180	1 [f]	2.7	0.650	0.507	0.005 [f]	91.0
vii	TPA^+	30	5.8	–	Na^+	179	25.4	2.7	1.07	0.559	0.135	86.0
viii	TPA^+	30	5.8	1	K^+	190	91.7	–	0.507	0.133	0.507	13.0
11-4	TPA^+	30	8.2	–	K^+	179	1 [f]	5.8	0.005	0.967	0.005 [f]	173
ix	TPA^+	30	8.2	–	Na^+	180	17.6	5.3	0.400	1.04	0.093	169
x	TPA^+	30	8.2	1	K^+	188	76.6	–	0.423	0.133	0.423	14.8
11-6	$TPMP^+$	30	5.8	–	K^+	180	21.7	2.0	0.400	0.256	0.115	40.4
xi	$TPMP^+$	30	5.8	–	Na^+	182	90.3	–	0.480	0.133	0.480	12.1
12-3	$TPMP^+$	30	5.8	1	K^+	183	136	–	0.700	0.133	0.700	6.18
11-5	$TPMP^+$	30	8.2	–	K^+	179	47.5	2.0	0.450	0.205	0.251	27.0
xii	$TPMP^+$	30	8.2	–	Na^+	179	40.8	–	0.213	0.133	0.213	18.3
12-5	$TPMP^+$	30	8.2	1	K^+	181	119	–	0.635	0.133	0.635	8.17
12-2, 12-4, 12-6	Same as 11-1, 11-6, and 11-5, respectively											

[a] Curves {10-1...12-6} are numbered T → B, then L → R in Figs. 10–12. Curves {i...xii} are from unplotted experiments. Curves {i, ii, viii} are from the same experiments as plotted curves {5-2, 5-4, and 5-6}, respectively, for LSI uptake. Symbols for concentrations, reaction constants, and flux are defined in the text for Eqs. (6)–(9).

[b] These values differ from the normalizing value of 180 mM (see legends to Figs. 10–12) in being best-fit estimates for Eq. (7)), dependent upon all of the data points in each plotted curve.

[c] The three reaction constants not listed here were calculated by fitting text Eq. (8) jointly to all of the independent single-component flux curves (those having no value of τ), with only a single parameter (k_{oc2}) not held in common. The resulting common parameter values ($k_{co0} = k_{co2} = 0.133$; $k_{oc0} = 0.961$) were then preset for fitting the two-component curves.

[d] Single-component curves are tabulated with no value of τ and with the corresponding '1' and '2' reaction constants equal.

[e] Alternative (bracketed) reaction constants were obtained by fitting Eq. (A – 3a) jointly to the point plots for 10-1, 10-2, and 10-5, but letting k_{co1}, rather than k_{oc1}, vary from curve to curve.

[f] The end concentration was fitted = 0 (see *c* in the legend table for Fig. 11), but was set here at a small finite value strictly for computation. These cells do not recover from LSI exposure.

LSI uptake, which could exceed 50 mM/min (Fig. 5 legend). But in the absence of added Ca^{2+}, much larger cation effluxes (> 75 mM/min) were often observed, which – particularly at high pH – significantly exceeded the measured cytosolic LSI influxes (Figs. 5,8 legends). Such independent variation of ion countermovements demonstrates their lack of obligatory coupling.

The two most predictable effects of high LSI concentrations upon cytoplasmic cation transport processes (effects clearly visible in the plots of Figs. 10 and 11) were a sudden increase of k_{co}, the specific rate constant for efflux, followed several minutes later by its recovery toward normal values (0.13). The increase varied from ~ 3- to 8-fold under different conditions (cf. Table 2, lines 10-6 and iv), with apparent recovery times (τ) of 2–6 min. The implied metabolic regulatory process was much faster than had been necessitated by electrophysiological data (Fig. 11, Ref. [1]).

LSI treatment also quickly diminished k_{oc}, the specific rate constant for cation influx. Except for an extreme case (Table 2, line 11-4), however, the relative effect on this parameter was smaller than upon k_{co}: from a control value of 0.96 (Table 2, footnote c) to ~ 0.2 (Table 2, line vi). And as expected from the fact that maintenance of the normal k_{oc} demands metabolic energy (i.e., active transport), no recovery of k_{oc} was observed in the sustained presence of LSI's; in fact, as required (Eq. (9d)) by the low value of C_{co} in many cases (c in Eq. (7)), k_{oc} fell further with sustained presence of LSI's. Several cases also appeared to be anomalous, with the best fits of Eq. (8) (specifically, Eqs. (A-3b) and (A-3d)) to the data yielding k_{oc} values ≥ the control value (Table 2, lines 10-3, 10-6, ii, iii). All of these cases involved Na^+-loaded cells, and the result suggests that the mechanism for Na^+ entry, in the absence of extracellular K^+, is very different from that for the active uptake of K^+ itself.

4. Discussion

There are few reports of biological experiments with lipid-soluble cations at concentrations above 1 mM, presumably because it has been known – since the first mitochondrial studies with these ions [17,18] – that they are concentrated in energy-converting organelles and act as uncoupling agents. Their most common use is as distribution probes for membrane voltage in small-cell systems, where applied concentrations are nearly always at or below (sometimes far below) 100 μM. Higher concentrations have been used with various artificial membrane preparations, as a way to modify bilayer dielectric properties or to study the physics of LSI transit through these model systems [19–21]. But while higher test concentrations have been reported in a few biological experiments [22–24], it seems likely that most such tests were made because experiments with lower concentrations had not 'worked', i.e., had not given the expected distribution ratios. That was, indeed, the initial reason for testing millimolar concentrations of TPP^+ and TPA^+ leading up to the present experiments.

However, the observation of a fairly rapid initial uptake of TPP^+ (> 10 mM/min) by *Neurospora* from extracellular concentrations of 100 μM, together with the brief equilibration time (< 2 min; Fig. 4, Ref. [1]) and with insult-induced refractoriness of the *Neurospora* membrane voltage to millimolar test concentrations (Fig. 11, Ref. [1]), led us to a more general examination of LSI uptake. We did not expect calcium ions to have such profound effects on LSI transport;

Table 3
Summary of initial fluxes induced in *Neurospora* by extracellular lipid-soluble cations

LSI concn.	0 calcium				1 mM calcium			
	LSI influx		H^+ efflux	$\{Na^+ + K^+\}$ efflux, J_{co0}	LSI influx	current	H^+ efflux	$\{Na^+ + K^+\}$ efflux, J_{co0}
	J_{oc0}	d	J_{co0}		J_{oc0}	ΔI_m	J_{co0}	
pH 5.8 ~								
2 mM	8.2	0.3	2.3	2.4	2.1	–	3.2	3.1
7 mM	42	3.8	−8.0 [a]	7.0	30	–	0.3	3.4
20–30 mM	82	8.2	−10	81	58	7–30	−6.3	10
pH 8.2 ~								
0.1 mM	16	< 0.1	–	–	–	–	–	–
2 mM	14	1.4	−1.1	0	1.3	–	–	3.5
7 mM	48	7.1	−0.6	10	20	–	−0.3	16
20–30 mM	190 [b]	25	−6.8	140	60	5–22	−5.6	15

Fluxes stated as mM/min, calculated as described in Materials and methods. Currents converted to flux units as discussed for Fig. 8, Ref. [1]. LSI fluxes for pH 5.8 summarized from Fig. 5; for pH 8.2 without calcium, from Fig. 8; for pH 8.2 with calcium, from data not shown; and for 0.1 mM TPP^+, from Ref. [1]. $\{Na^+ + K^+\}$ fluxes averaged from Table 2, col. 13. TPP^+ in most experiments, TPA^+ in a few. J_{oc0} includes values of d, the linear component of LSI uptake.

[a] Negative sign here signifies apparent H^+ influx, or OH^- efflux.

[b] Value corrected for entry of TPP^+ into the putative parallel (extracellular) compartment.

neither did we expect an intracellular sub-compartment (Figs. 7 and 9) to sequester a major fraction of the LSI taken up; nor did we expect to have so much difficulty accounting for the charge balance.

4.1. Synopsis of LSI uptake

The main features of LSI uptake which can be culled from Figs. 5–9 above, and Figs. 4, 5 of the previous paper, are the following: (i) Uptake curves at millimolar LSI concentrations are described by two flux components: a fast one having a (common) single-exponential time constant (α), and a slower linear one (d). (ii) 1 mM calcium blocks the linear component of LSI entry, but reduces the fast component much less, about 40% at the higher concentrations, and 80% at 2 mM. (iii) A significant effect of pH_o on LSI influx occurs only in the absence of extracellular Ca^{2+}, and is subtle: mainly changing the kinetic order (Hill coefficient $n = 1$ at pH 8.2, but $n = 2$ at pH 5.8; see Fig. 9). (iv) The measured influx from micromolar $[TPP^+]_o$ is much faster ($\sim$ 15 mM/min at 100 μM) than would be inferred from the concentration dependence at millimolar LSI concentrations (< 1 mM/min extrapolated from Fig. 9B, at pH 8.2), but *in extent* never reaches electrochemical equilibrium. (v) More generally, the fast component of LSI uptake from millimolar concentrations may reach apparent electrochemical equilibrium, but does not exceed it (except see pH 8.2 with 20 mM $[TPP^+]_o$, Fig. 8A). vi) However, the slow component – absent extracellular Ca^{2+} – does go beyond the apparent electrochemical equilibrium (Fig. 8A,B) after 10–15 min, even when calculated on the basis of total cytoplasmic volume. Numerical values for the LSI influxes under various conditions are summarized in Table 3 (columns 2,3,6).

4.2. Possible ion counterfluxes

Simple electrophoretic uptake of lipid-soluble cations, the postulated transport mechanism in liposomes, animal cells, and Gram-positive bacteria, would require a balancing (stoichiometric) current of the other ions which normally support the resting membrane voltage of the organism. In the case of *Neurospora*, that should be mainly H^+ ions, driven outward through the plasma-membrane proton ATPase and short-circuited by the conductance due to lipid-soluble ions. Satisfactory electrical measurements are possible only at the higher LSI concentrations (e.g., Fig. 8, Ref. [1]) in the presence of 1 mM $[Ca^{2+}]_o$, and those yield estimates of LSI-induced currents between 10% and 50% of the pertinent LSI influxes (Table 3, column 7). The implied net H^+ effluxes, however, are either missing or almost totally masked (Figs. 1–3; summarized in Table 3, columns 4,8), thus leaving unresolved two fundamental questions about LSI transport: the physical mechanisms for LSI entry and for maintenance of macroscopic electroneutrality.

More complex devices for ion exchange (i.e., carrier-mediated exchange) can be postulated to admit other ion fluxes into the charge-balance equation, with obvious candidates being the normally predominant cytoplasmic cations, Na^+ and K^+. LSI-induced movements of these ions (Figs. 10–12) proved to be at least as complex as those of TPP^+ or TPA^+, but are kinetically very distinct. Furthermore, only under one condition: at the highest LSI-concentrations tested, and in the absence of extracellular Ca^{2+}, are effluxes of these ions large enough to balance (roughly) the measured LSI influxes (see Table 3, column 5).

4.3. Additional inferences

The net conclusion of results summarized in Table 3 is that uptake of lipid-soluble cations (specifically TPP^+ and TPA^+) from millimolar extracellular concentrations can occur largely independently of the expected or likely cellular ion-exchange mechanisms. Then either or both of the following must occur: entry of extracellular anions in an electroneutral complex with the lipid-soluble cations, or exit of organic cations.

Furthermore, as noted in item (vi) above, the slow-phase accumulation of TPP^+ or TPA^+ reaches concentrations beyond electrochemical equilibrium. This finding *absolutely necessitates compartmentation* – either chemical or structural – of the excess LSI's. But if physical compartmentation does occur, then the actual concentrations of LSI's reached in the so-called storage compartment (Fig. 6; Eq. (5)) would be further increased, by the ratio of total intracellular volume to the storage volume. There are three likely anatomical loci for storing lipid-soluble cations in fungal cells: (a) intracellular membranes themselves, by oil-water partitioning; (b) polysaccharide storage granules common in fungal cytosol; and (c) the vacuolar space, where lipid-soluble cations could be electrostatically bound into storage polyanions [25–27]. For the major factor, we favor sequestration in the vacuolar space, and posit the following overall hypothesis, which leads to several simple testable predictions.

4.4. Hypothesis

(1) The major mode of entry of lipid-soluble ions, such as TPP^+ and its congeners, into fungal cells is by electroneutral diffusion in combination with one or more conventional anions (in the present experiments, OH^-, Cl^-, Br^-, $H_2PO_4^-$, HPO_4^{2-}, $Hepes^-$, Mes^-, DMG^{2-}, $HDMG^-$, H_2Cit^-, $HCit^{2-}$).

(2) Slower diffusion of the neutral complexes occurs within the cytoplasm, resulting in penetration of organellar spaces, particularly the vacuolar space.

(3) Within the vacuolar space, the lipid-soluble cations bind to storage polyanions, chiefly polyphosphate, which can provide neutralizing charge concentrations as high as 1 M or more, with low osmotic activity [25,26].

(4) Anions released from the diffusible LSI complexes combine with cations released from polyphosphate (e.g., K^+, Na^+, basic amino acids, polyamines [26,27]) and redistribute to the cytoplasm and the cell exterior, depending on many factors.

(5) Escape of basic amino acids and polyamines to the cell exterior accounts for the apparent acid influx which accompanies LSI uptake by *Neurospora*.

Although it is not integral to the hypothesis, we view the LSI-induced losses of $\{Na^+ + K^+\}$ from *Neurospora* (Figs. 10–12) as secondary consequences of deranged energy metabolism (e.g., disruption of mitochondrial function). Except in extreme cases, however, membrane control mechanisms are able to 'limit the damage' by tightening the membrane after an initial rush of ion loss, thus conferring rather complicated efflux kinetics. Understanding of these processes requires conceptual dissociation from LSI influxes per se, and Eqs. (8), (9), (A-1)–(A-3) provide useful independent descriptive tools.

4.5. Testable predictions

(1) The activity coefficients of lipid-soluble cations in aqueous solution should depend strongly on the nature of accompanying anions, and the osmotic effects of LSI-salt solutions should vary accordingly.

(2) The slow component of LSI uptake by *Neurospora* should be enhanced in both speed and magnitude by maneuvers which increase vacuolar volume. One such maneuver is simple carbon starvation [28].

(3) Since extracellular Ca^{2+} retards or may even block transfer of cytoplasmic LSI's into the storage compartment, $[Ca^{2+}]_o$ must affect vacuolar (tonoplast) permeability. That would occur most simply if $[Ca^{2+}]_c$ were to rise with extracellular concentration, at least under the conditions of these experiments.

(4) The LSI's tested (TPP^+, TPA^+, $TPMP^+$) should bind strongly to polyphosphate, in in-vitro experiments.

(5) TPP^+ and TPA^+ should elicit substantial losses of basic amino acids and/or polyamines both from isolated vacuoles and from intact cells of *Neurospora*.

5. Appendix

Formally, the ensemble 'pump-leak' model for membrane transport (Fig. 6B) can be stated as

$$\frac{dC_c}{dt} = C_o k_{oc} - C_c k_{co} \tag{A-1a}$$

and

$$\frac{dC_o}{dt} = -C_o k_{oc} + C_c k_{co} \tag{A-1b}$$

where the rate 'constants' k_{oc} and k_{co} are usually presumed to be fixed, time-independent parameters. In the particular geometry of these experiments (see also text leading to Eqs. (3)–(5)), with extracellular volume sufficiently large to keep C_o constant throughout any one experiment, the second differential equation above drops out, and the first has the elementary solution

$$C_c = \left(C_{cs} - \frac{k_{oc}}{k_{co}} C_o\right) e^{-k_{co}t} + \frac{k_{oc}}{k_{co}} C_o \tag{8}$$

in which C_{cs} is the starting value of $[Na^+ + K^+]_c$ and must be different from the stable value $(C_o \cdot k_{oc}/k_{co})$ once the rate constants have been reset by the experimental treatment. The cytoplasmic ion content varies as a single exponential in time, with a rate constant which is characteristic for *efflux* from the cytoplasm (and which conceals a term for cytoplasmic volume).

Since Eq. (8) contains only a single rate constant in the time-dependence term, the second *observed* phase of cation efflux must arise from another process; that is, either k_{oc} or k_{co} must vary with time. The general differential equation for this case:

$$\frac{dC_c(t)}{dt} = C_o \cdot k_{oc}(t) - C_c(t) \cdot k_{co}(t) \tag{A-2}$$

where (t) explicitly designates time-dependent variables, can be solved in terms of the exponential integral when k_{oc} and k_{co} are simple exponential functions. But the solutions are cumbersome and not justified by the quality and quantity of data represented in Figs. 10–12.

A simpler procedure, and one more informative for present purposes, is piecewise application of Eq. (8) for two intervals: that immediately following addition of LSI to the cell suspension ($t = 0$), and that following cellular adaptation to the LSI ($t = \tau$). This approximates the slower or delayed effect of LSI on $\{Na^+ + K^+\}$ fluxes as a sudden change, rather than as a gradual change. Then the following relationships can be written from Eq. (8) (nomenclature for the rate constants is given in the main text):

$$t = 0: \qquad C_c = C_{cs} = \frac{k_{oc0}}{k_{co0}} C_o \tag{A-3a}$$

$$0 < t < \tau: \quad C_c = C_o\left(\frac{k_{oc0}}{k_{co0}} - \frac{k_{oc1}}{k_{co1}}\right) e^{-k_{co1}t} + \frac{k_{oc1}}{k_{co1}} C_o \tag{A-3b}$$

$$t = \tau: \qquad C_c = C_{c\tau}$$

$$= C_o\left(\frac{k_{oc0}}{k_{co0}} - \frac{k_{oc1}}{k_{co1}}\right) e^{-k_{co1}\tau} + \frac{k_{oc1}}{k_{co1}} C_o \tag{A-3c}$$

and

$$t > \tau: \qquad C_c = \left(C_{c\tau} - \frac{k_{oc2}}{k_{co2}} C_o \right) e^{-k_{co2}(t-\tau)} + \frac{k_{oc2}}{k_{co2}} C_o \qquad \text{(A-3d)}$$

In this sequence, Eqs. (A-3a) and (A-3c) represent the initial values of C_c for the subsequent intervals, and Eqs. (A-3b) and (A-3d) represent the continuous change of C_c over those intervals.

Two additional relationships are needed to extract all of the parameters in Eqs. (A-3) from the data and fits to the empirical function of Eq. (7). The simplest ones – both in terms of mathematics and in terms of biological effects – come from assuming (a) that in the presence of extracellular calcium (1 mM), LSI's have very little effect on the *efflux* rate constant; i.e., $k_{co2} = k_{co1} = k_{co0}$; and (b) that adaptation (the delayed effect) returns k_{co} approximately to its control value, whether or not Ca^{2+} is present; i.e., $k_{co2} \approx k_{co0}$, even when $k_{co1} \gg k_{co0}$. These assumptions simply restate the empirical observation (Figs. 10–12) that the slow phase of cation efflux has approximately the same rate constant under all conditions tested (that is, Eq. (7) can be fitted to all of the data with a single common value of β). Thus, the slow-phase efflux is interpreted as a secondary down-shift of permeability, roughly compensating for the LSI-induced increase.

6. Acknowledgements

Supported by research grant FG02-8 ER13359 from the U.S. Department of Energy and GM-15858 from the National Institute of General Medical Sciences (C.L.S.); by a Fogarty Fellowship (A.B.-D.); by the National Research Council of Italy, Spec. Proj. RAISA, Subproj. 2 (A.B.-D.); and by sabbatical funds from Aichi-Gakuin University, Nagoya (H.K.). The authors are indebted to Ms. Sue Shannon and Dr. Esther Bashi for expert technical assistance and to Dr. H.R. Kaback (University of California at Los Angeles) for tritiated TPP^+ and TPA^+.

7. References

[1] Ballarin-Denti, A., Slayman, C.L. and Kuroda, H. (1994) Biochim. Biophys. Acta 1190, 43–56.
[2] Slayman, C.L., Long, W.S. and Lu, C.Y.-H. (1973) J. Membr. Biol. 14, 305–338.
[3] Slayman, C.L. (1977) in Water Relations in Membrane Transport in Plants and Animals (Jungreis, A.M., Hodges, T.K., Kleinzeller, A. and Schultz, S.G., eds.), pp. 69–96, Academic Press, New York.
[4] Gradmann, D., Hansen, U.-P., Long, W.S., Slayman, C.L. and Warncke, J. (1978) J. Membr. Biol. 39, 333–367.
[5] Slayman, C.L. (1980) in Plant Membrane Transport: Current Conceptual Issues (Spanswick, R.M., Lucas, W.J. and Dainty, J., eds.), pp. 179–190, Elsevier/North-Holland, Amsterdam.
[6] Rodriguez-Navarro, A., Blatt, M.R. and Slayman, C.L. (1986) J. Gen. Physiol. 87, 649–674.
[7] Slayman, C.L. and Slayman, C.W. (1968) J. Gen. Physiol. 52, 424–443.
[8] Marquardt, D.W. (1963) J. Soc. Ind. Appl. Math. 11, 431–441.
[9] Slayman, C.W. and Slayman, C.L. (1970) J. Gen. Physiol. 55, 758–786.
[10] Dijkshoorn, W. (1962) Nature 194, 165–7.
[11] Imsande, J. (1986) J. Exp. Bot. 37, 341–347.
[12] Conway, E.J. and Breen, J. (1945) Biochem. J. 39, 368–371.
[13] Armstrong, W.McD. and Rothstein, A. (1964) J. Gen. Physiol. 50, 967–988.
[14] Roon, R.J., Even, H.L., Dunlop, P. and Larimore, F. (1975) J. Bacteriol. 122, 502–509.
[15] Blatt, M.R., Rodriguez-Navarro, A. and Slayman, C.L. (1987) J. Membr. Biol. 98, 169–189.
[16] Slayman, C.W. and Tatum, E.L. (1964) Biochim. Biophys. Acta 88, 578–592.
[17] Grinius, L.L., Jasaitis, A.A., Kadziauskas, Y.P., Liberman, E.A., Skulachev, V.P., Topali, V.P., Tsofina, L.M. and Vladimirova, M.A. (1970) Biochim. Biophys. Acta 216, 1–12.
[18] Bakeeva, L.E., Grinius, L.L., Jasaitis, A.A., Kuliene, V.V., Levitsky, D.O., Liberman, E.A., Severina, I.I. and Skulachev, V.P. (1970) Biochim. Biophys. Acta 216, 13–21.
[19] Levine, B.A., Sackett, J. and Williams, R.J.P. (1979) Biochim. Biophys. Acta 550, 201–211.
[20] Ruifrok, P.G. and Meijer, K.F. (1981) Naunyn-Schmied. Arch. Pharmacol. 316, 266–272.
[21] Bühler, R., Stürmer, Apell, H.-J. and Läuger, P. (1991) J. Membr. Biol. 121, 141–161.
[22] Cerana, R., Bonetti, A., Colombo, R. and Lado, P. (1981) Planta 152, 202–208.
[23] Ritchie, R.J. (1984) J. Exp. Bot. 35, 699–706.
[24] Gibrat, R., Barbier-Brygoo, H., Guern, J. and Grignon, C. (1985) Biochim. Biophys. Acta 819, 206–214.
[25] Cramer, C., Vaughn, L.E. and Davis, R.H. (1980) J. Bacteriol. 142, 945–952.
[26] Cramer, C. and Davis, R.H. (1984) J. Biol. Chem. 259, 5152–5157.
[27] Davis, R.H. and Rostow, J.L. (1991) Arch. Biochem. Biophys. 285, 306–311.
[28] Moussatos, V.V. and Slayman, C.L. (1993) Plant Physiol. 102 (Suppl.), 109 (Abstr. No. 615).